Available online at www.jourcc.com

Journal homepage: www.JOURCC.com

Journal of Composites and Compounds

Functionalized $NiFe_2O_4$/mesopore silica anchored to guanidine nanocomposite as a catalyst for synthesis of 4H-chromenes under ultrasonic irradiation

Somaye Mohammadi [a]*, *Zeinab Mohammadi* [a]

[a] *Department of Organic Chemistry, Faculty of Chemistry, University of Kashan, Kashan, 87317-51167, I.R. Iran; Tel: 98-31-55912388; Fax: 983155912397*

ABSTRACT

A synergetic effect of nanocatalyst and ultrasonic irradiation was examined for the synthesis of 4H-chromenes from benzaldehyde, cyclohexanone, and malononitrile. It was observed this contributory improved the reaction that was used for the synthesis of the highly pure products in short reaction times and highest yields. The nanocomposite includes the guanidine anchored on to magnetic $NiFe_2O_4$ nanoparticles were used as the active base nanocatalyst for the sonication synthesis of 4H-chromenes compounds. The product was separated with simple filtration and purify with recrystallization by ethanol solvent. After completing the reaction, a nanocatalyst was collected and reused in 6 runs of model reaction. This nanocomposite has a magnetic core and a very active base surface area shell. The nanocatalyst was provided by the simple technique and identified by using FT-IR spectrum, scanning electron microscopy (SEM), X-ray diffraction (XRD), vibrating sample magnetometer (VSM), and Brunauer–Emmett–Teller (BET). This nanocomposite was used for the synthesized various derivatives of 4H-chromenes under ultrasonic irradiation. The organic products were identified by FT-IR and 1H-NMR.

Peer review under responsibility of JCC Research Group

ARTICLE INFORMATION

Article history:
Received 07 March 2021
Received in revised form 12 April 2021
Accepted 26 May 2021

Keywords:
4H-Chromene
Cyclohexanone
Malononitrile
Ultrasonic mesopore silica

1. Introduction

Recently mesoporous silica spheres include magnetic metal nanoparticles, have an attractive idea for chemistry researchers [1-3]. These nanocomposites have active surfaces area for use in various sciences. This nanostructure has the potential for use as the nanocatalyst [4-6], sensors [7, 8], nanoreactors [9], and drug delivery processes [10], gas filtration [11], and also as nano-sized quantum materials [12]. The large surface area of mesoporous silica was used in optical coatings and catalytic processes [13]. The bulk mesophase [14, 15] was managed the ratio between silica-to-surfactant and silica/surfactant self-assembly formation of cubic, hexagonal, and lamellar shape [16]. Recently, the heterogeneous nanocomposite was used in organic reaction to synthesis of different organic products [17, 18].

The chromenes compounds have notable biological attributes, [19-21] such as anticancer [22], antibacterial [23], anticonvulsant [24], antimicrobial [25], anti-influenza [26], antimalarial [27], and anti-virus activities [28]. Tetrahydro-4H-chromenes were used for the cure of counting Huntington's disease [29] neurodegenerative illnesses [30], Alzheimer's disease [31], Parkinson's disease [32], and schizophrenia [33]. The usual reaction for synthesis tetrahydro-4H-chromene is the Michael addition in the presence of a base catalyst. Numerous multi-component reactions have been determined for the synthesis of various tetrahydro-4H-chromenes derivatives via the condensation of an aldehyde, malononitrile, and cyclic ketone at the presence of different inorganic and organic catalysts [33, 34].

Ultrasonic is the sound waves belonging to the group of mechanical waves, which included frequencies higher than the audible frequency of humans (20k Hz) [35, 36]. The piezoelectric influence has been used to provide ultrasonic waves since the 1880 s [37, 38]. Ultrasonic waves were invented with development in the technology of ceramic materials [39], for example, quartz, [40] lead zirconate barium titanate, and lead titanate [41, 42], the ultrasonic technique has progressively grown to be considered encouraging, green, and novel technology that can be replaced or help traditional chemical processing [43, 44].

Following the previously reported [45-47], in this research, it was reported a clean synthesis of 4H-chromenes derivatives from cyclohexanone, different benzaldehyde, and malononitrile under ultrasonic irradiation at the presence of the $NiFe_2O_4$/mesopore silica anchored to guanidine nanocomposite as the base catalyst.

* *Corresponding author: Somaye Mohammadi; E-mail:mohamadi_s65@yahoo.com*
DOR: 20.1001.1.26765837.2021.3.7.1.6
https://doi.org/10.52547/jcc.3.2.1

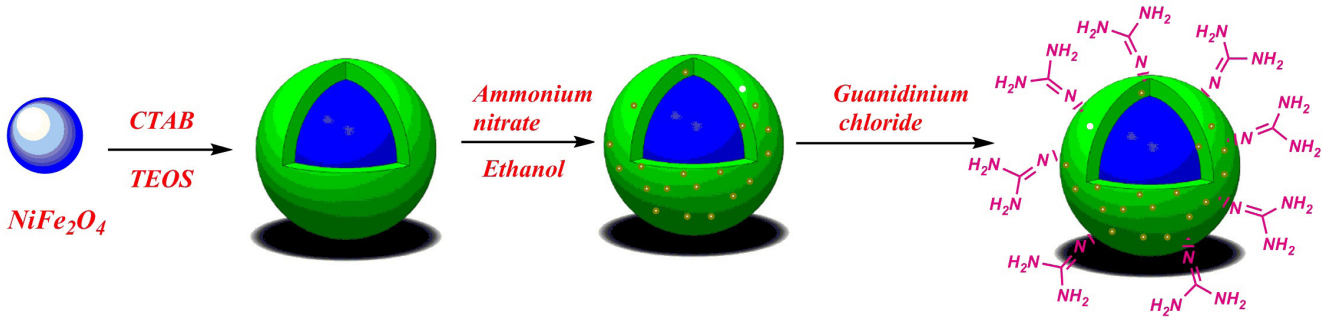

Scheme. 1. Synthesis of $NiFe_2O_4$/mesopore silica anchored to guanidine nanocomposite.

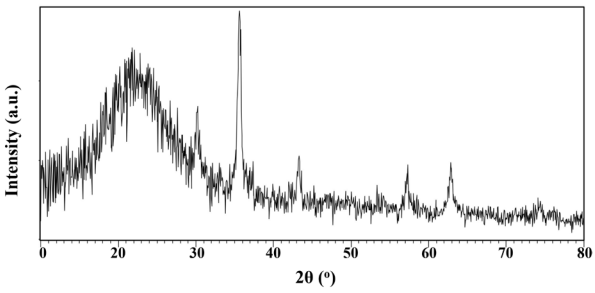

Fig. 1. XRD spectra of $NiFe_2O_4$@mesopore silica@ guanidine.

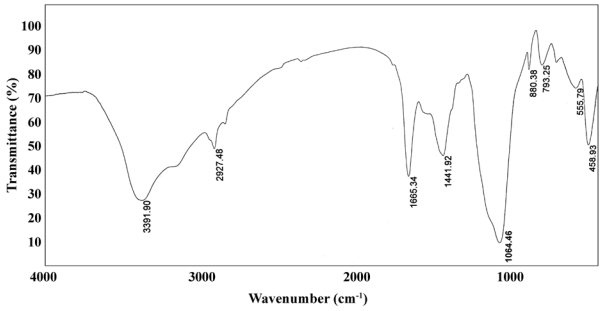

Fig. 2. The spectra of FT-IR of $NiFe_2O_4$@mesopore silica@ guanidine.

2. Experimental procedures

2.1. Materials and instruments

All the solvents and starting materials that used in the reaction include benzaldehyde derivatives (97%-99%), cyclohexanone (98%), malononitrile (99%), and ethanol (99%), cetyltrimethylammonium bromide (CTAB) (100%), tetraethyl orthosilicate (TEOS) (97%), sodium hydroxide (NaOH) (99%), were provided from Sigma, ferric (III) chloride ($FeCl_3$) (97%), nickel (II) chloride ($NiCl_2$) (98%), and sodium bicarbonate (95%), were obtained from Sinopharm Chemical. The organic products were recognized with ^1H NMR, FT-IR, and ^{13}C NMR analyses. The 1H NMR analysis was reported in $CDCl_3$ solvents using Bruker DRX-400 spectrometer, and the internal reference is tetramethylsilane. FT-IR spectra were reported with a Perkin-Elmer 550 spectrometers in the range of 400–4000 cm^{-1}. The crystal structure of nanocomposite (XRD) registered with (CuKa, radiation, λ = 0.154056 nm) that worked with a 15-kV accelerating voltage at the speed of 2° min−1 starting from 10° to 80°(2z.Theta;), for determined the morphology and size of nanocomposite used of Electron Microscope (FE-SEM) and EDX with Zeiss Scanning Electron with a 15-kV accelerating voltage. The surface areas and the size of pore in the nanocomposite illustrated by BET analysis with nitrogen adsorption in −196 °C using Tri-Star 3020 Micrometrics analyzer. The magnetic properties of nanocomposite were measured by a vibrating sample magnetometer (VSM), the VSM curves were recorded by PPMS-9 T at 300 K. The TGA was recorded in an air atmosphere by a 10 °C/min rate.

using the METLER-810 analyzer.

2.2. General procedure for preparation of nano magnetic $NiFe_2O_4$

The nickel ferrite nanoparticles were provided during a sol-gel method [29]. To the accomplishment, the chemical formula $NiFe_2O_4$, 40 ml $FeCl_3$ 6 H_2O (4 M) was stirred with 40 ml $NiCl_2$ $2H_2O$ (2 M). Then, 1.5 g citric acid monohydrate was added ($C_6H_8O_7$, H_2O) to the reaction mixture. The pH of the mixture increased to 7.0 added a little ammonia-water (NH_3-H_2O) to the reactions. The solution was heated to dry the water at 85°C and production of the brown colored gel. At the end of the method, the product was dry at 800 oC to 3h.

2.3. Synthesis of $NiFe_2O_4$@ mesopore silica

To provide an active base nanocatalyst, 5 mL NaOH 1 M, and 0.65 g of CTAB were dissolved in 100 mL deionized water and heated the mixture to 35 min at 100 °C. Then 0.1 g of $NiFe_2O_4$ nanocomposite was dispersed in 60 ml ethanol under sonicate irradiation. The obtained solution added to the reaction mixture. 2 ml TEOS was added to the reaction mixture two times after 15 and 40 min, the reaction mixture stirred at room temperature for 15 h at the end of the reaction the product collected by centrifuge and washed three times with water and ethanol, and dried at 70 °C for 24 h. The surfactant was removed from the nanocomposite by dispersed the product in ethanol (100 mL) and ammonium nitrate (50 mg) and stirred at 80 °C for 5 h. The product was separated by the centrifuge and dried at 100 °C for overnight.

2.4. Synthesis of $NiFe_2O_4$/mesopore silica anchored to guanidine nanocomposite

50.0 mg of $NiFe_2O_4$@mesopore silica was dispersed under ultrasonic irradiation in 10.0 mL toluene solvent for 30 min. Then 5mmol guanidinium chloride, 5 mmol 3-chloropropyltrimethoxysilane, and 2.5 mmol sodium bicarbonate in 10 mL dry toluene added to the reaction mixture then refluxed for 32 h. Then, the final product was separated by centrifuge and washed with water and ethanol. The product was dried at 80 °C under a nitrogen atmosphere (Scheme 1).

2.5. General multicomponent procedure for synthesis of 4H-chromene

4H-chromenes derivatives were synthesized in the three-component reaction. In this reaction, 1 mmol of malononitrile was reacted by 1 mmol of benzaldehyde at the presence of 10 mg of nanocatalyst. The reaction was followed under ultrasonic irradiation on the ethanol

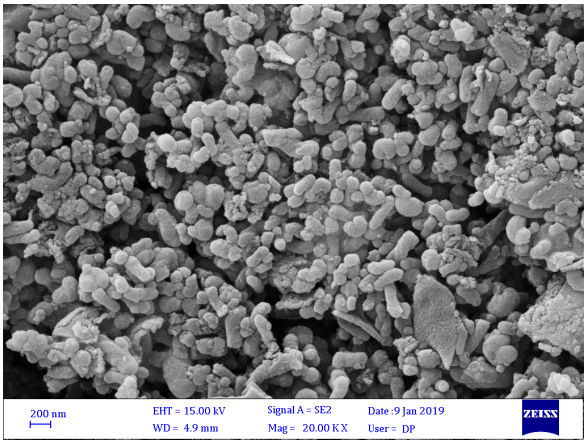

Fig. 3. FE-SEM image of $NiFe_2O_4$@mesopore silica@ guanidine.

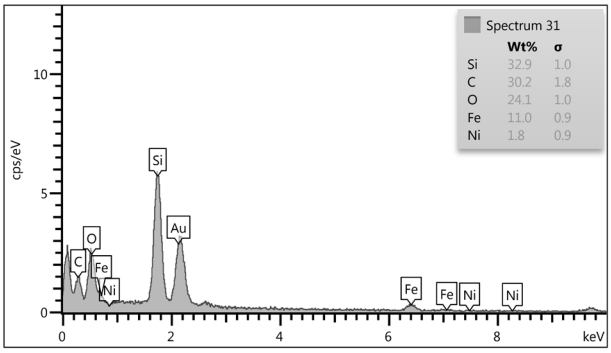

Fig. 5. EDS curves for $NiFe_2O_4$@mesopore silica@ guanidine.

solvent. After 5 min 1 mmol cyclohexanone was added to the reaction mixture, and the process was followed by thin-layer chromatography. The final product was separated with simple filtration and purification by recrystallization in the ethanol solvent. The final product identifies by the melting point, FT-IR, and ^{1}H NMR spectra (^{1}HNMR and FT-IR data were placed in SI files).

3. Result and discussion

3.1. Preparation and characterization

The $NiFe_2O_4$ nanoparticles were synthesized and functionalized by mesopore silica and guanidine. At first, $NiFe_2O_4$ was provided by the sol-gel method [48]. The obtained $NiFe_2O_4$ was reacted by CTAB, NaOH, and TEOS at ambient temperature to $NiFe_2O_4$ @ mesopore silica. The obtained magnetic nanocomposites reacted by guanidine under the refluxed condition to $NiFe_2O_4$@mesopore silica@ guanidine base nanocatalyst. The nanocomposite was distinguished by various analyses

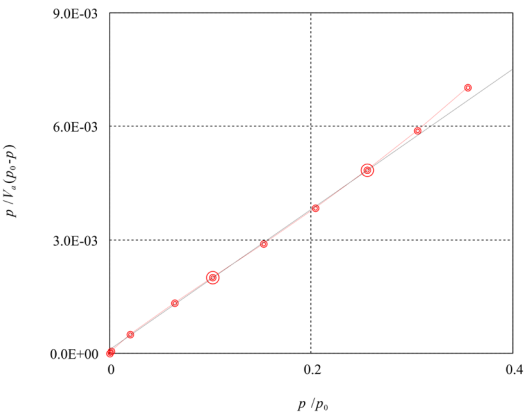

Fig. 4. BET curves for $NiFe_2O_4$@mesopore silica@ guanidine.

such as; SEM, EDX, XRD, FT-IR, BET, and VSM.

The XRD models were recorded of the crystal structure of $NiFe_2O_4$@ mesopore silica@ guanidine displayed in Fig. 1. The XRD pattern in Fig 1 shows the peaks (miller indices) in 30° (220), 37° (222), 45° (400), 58° (511), 62° (440) and 73°(533), regular XRD pattern of JCPDS card that due to the crystal structure of$NiFe_2O_4$ and the sharp peak in 22° due to amorphous mesopore silica.

Effective functionalization of the $NiFe_2O_4$@mesopore silica@ guanidine catalyst can be explained through FT-IR spectra (Fig. 2). According to the FT-IR spectrum of the nanocomposite, the presence of a peak around 458 cm^{-1} showed stretching vibration of Ni-O bonding; the peak of Fe-O looked near the 793 cm^{-1}; the NH^2 stretching bond displayed near 3391 cm^{-1}, and the peak of the Si-O stretching bond appeared around 1084 cm^{-1}.

The morphology and size of the nanocomposite were defined by the scanning electron microscopy analysis. The FE-SEM images of the $NiFe_2O_4$@mesopore silica@ guanidine (Fig. 3) shown the extremely uniform morphology for the nanocomposite. Moreover, the average particle size of $NiFe_2O_4$@mesopore silica@ guanidine was 77-85 nm.

The surface area and pore volume diameter of $NiFe_2O_4$@mesopore silica@ guanidine were defined using the Brunauer–Emmett–Teller (BET) technique. According to the acquired curve, the measurement of surface area was equal to 233 m_2g_{-1}, total pore volume 0.121 cm^3g^{-1} (Fig. 4).

Also, to characterize the percent of each element in the nanocomposite, it was studied elemental the energy-dispersive X-ray (EDS) spectrum. The EDS curve showed the percent of O, Si, Fe, Ni, and C were 24.1%, 32.9%, 1.8%, and 30.2`%, respectively (Fig. 5).

Thermogravimetric analysis (TGA) curves (Fig. 6) of $NiFe_2O_4$@ mesopore silica@ guanidine shows that losses of 60 percent of weight under 800 °C in the models are due to the release of adsorbed water, solvent, and organic materials.

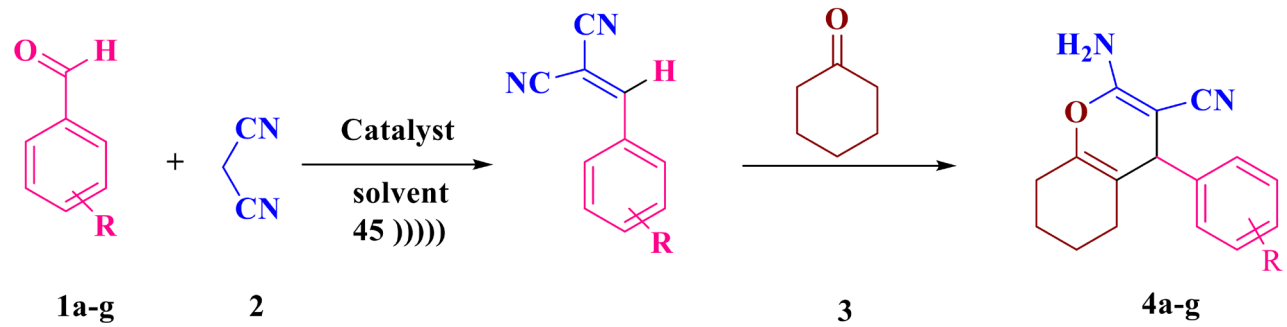

Scheme. 2. Synthesis of various derivatives of 4H-chromene in the presence of $NiFe_2O_4$/mesopore silica/guanidine nanocatalyst.

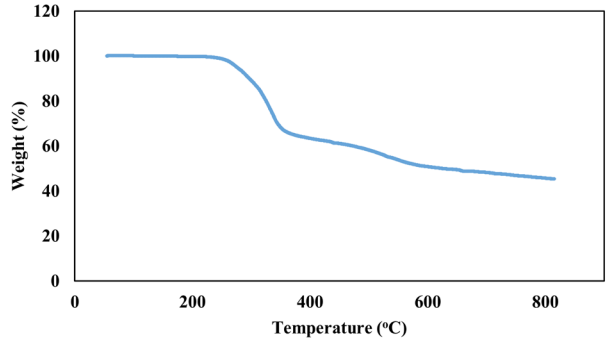

Fig. 6. TGA curves for $NiFe_2O_4$@mesopore silica@ guanidine.

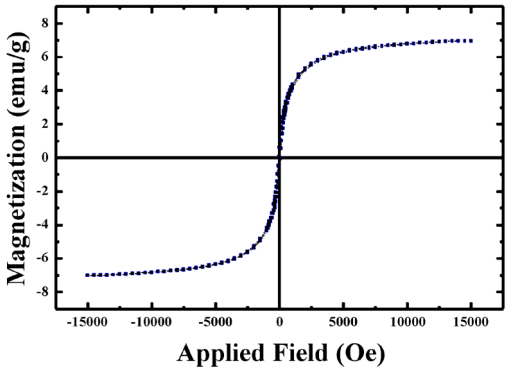

Fig. 7. FVSM curves for $NiFe_2O_4$@mesopore silica@ guanidine.

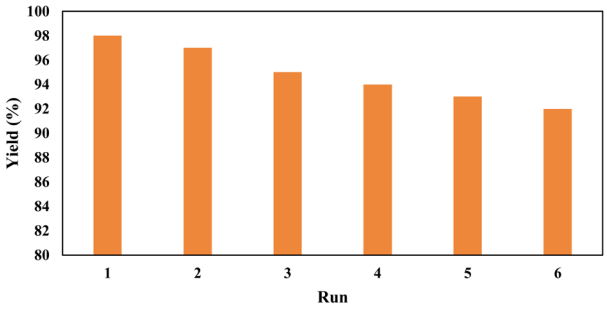

Fig. 8. The recyclability of $NiFe_2O_4$/mesopore silica/guanidine nanocatalyst in six runs.

Table 1.
Investigation of catalyst, catalyst amount in ethanol solvents for the synthesis of 4H-chromenes [a]

Entry	Catalyst	Catalyst amount (mg)	Time (h)	Yield [b] (%)
1	Et_3N	10	3.5	40
2	MgO	10	2.5	70
3	Morpholine	10	0.95	70
4	Guanidine	10	0.75	75
5	$NiFe_2O_4$/mesopore silica/guanidine	10	0.75	88
6	$NiFe_2O_4$/mesopore silica/guanidine	10	0.16	98
7	$NiFe_2O_4$/mesopore silica/guanidine	5	0.16	83
8	$NiFe_2O_4$/mesopore silica/guanidine	15	0.16	90

[a] Reaction conditions: benzaldehyde (1 mmol), malononitrile (2 mmol), cyclohexanone (1 mmol), 5 ml solvent.
[b] Isolated yield

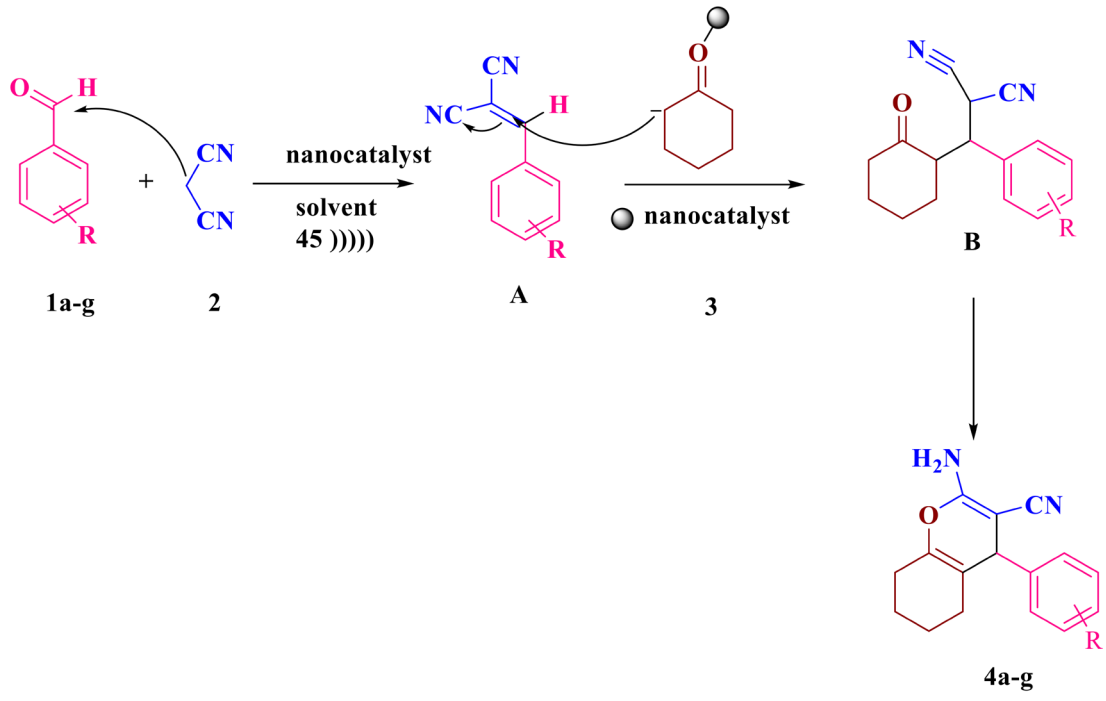

Scheme. 3. Proposed reaction mechanism for the Synthesis of 4H-choromene.

Table 2.
Investigation of solvent for the synthesis of 4H-chromenes [a]

Entry	Solvent	T °C	Time (h)	Yield [b] (%)
1	Acetonitrile	25	0.75	10
2	Chloroform	25	0.92	0
3	Ethanol	75	0.16	98
4	Methanol	25	0.75	90

[a] Reaction conditions: benzaldehyde (1 mmol), malononitrile (2 mmol), cyclohexanone (1 mmol), 5 ml solvent.
[b] Isolated yield

The magnetic properties of $NiFe_2O_4$@mesopore silica@ guanidine nanocomposite were recorded by the vibrating sample magnetometry (VSM) spectra of the nanocomposite. The magnetization curve of nanocomposite shown superparamagnetic properties (Fig. 7).

According to the TGA and EDX analyzed, the percent of organic materials was 60%, and mesopore silica around 30%. So, the percent of $NiFe_2O_4$ is around 10% in the nanocatalyst structure. Because the low percent of $NiFe_2O_4$ and covered with two-layer of mesopore silica and guanidine compound. The MS of the catalyst was decreased, but it has superparamagnetic properties and adsorbed with an external magnet.

The synthetic reaction of 4H-chromenes from benzaldehyde, cyclohexanone, and malononitrile was optimized by various solvents, catalysts, and temperatures.

The reaction was studied by utilizing different catalysts such as morpholine, Et_3N, MgO, and $NiFe_2O_4$/mesopore silica/guanidine in the ethanol solvents. The results of the study were exhibited in Table 1.

The results were displayed $NiFe_2O_4$/mesopore silica/guanidine (Table 1, Entry 5) and have the best yields of product in the short reaction time. The model reaction was tested in different solvents and the result showed in Table 2.

Table 3.
Several Power for the ultrasonic multicomponent reaction for synthesis of bis-ortho-aminocarbonitrile tetrahydronaphthalene 4a [a]

Entry	Power (W)	Time (min)	Yield [b] (%)
1	Silent	180	20
2	30	60	82
3	35	50	85
4	40	35	90
5	45	10	98
6	50	30	96

[a] Reaction conditions: Benzaldehyde (1 mmol), Cyclohexanone (1 mmol), Malononitrile (1 mmol), 5 ml Solvent.
[b] Isolated yield

Ultrasound irradiation was constructed as the motive energy for the improved yield of 4H-chromenes, that due to the increased temperature correlated to the production of hot spots. While the reaction was carried out without sonic irradiation in low yield and long reaction time (Table 3, entry 1). The best power for the reaction was acquired 45 W based on product yield and reaction time (Table 3, entry 5).

After optimization of the model reaction for the synthesis of 4h-chromene (4a-g), 1 mmol of benzaldehyde (1a-g), 1 mmol of malononitrile **(2)**, and 1mmol of cyclohexanone (3) were mixed in ethanol solvent and 5 mg $NiFe_2O_4$/mesopore silica/guanidine added to the mixture as the base nanocatalyst. The reaction was done under 45 power ultrasonic irradiation (Scheme 2) (Table 4).

The mechanism of the reaction for the production of 4H-chromenes

Table 4.
Synthesis of various derivatives of 4h-chromene in the presence of $NiFe_2O_4$/mesopore silica/guanidine nanocatalyst [a]

4a-l [a], yield % [b], Time (min)		
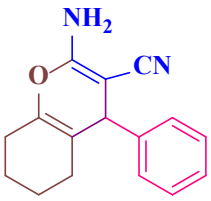 **4a: X= H, Y= H, 98, 10**	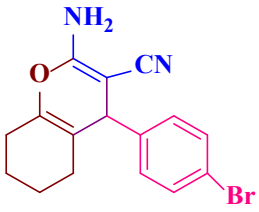 **4b: X= Br, Y= H, 95, 15**	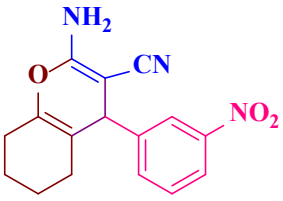 **4c: X= NO_2, Y= H, 96, 16**
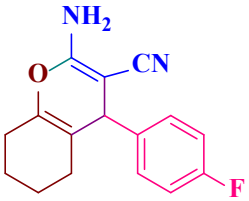 **4d: X= F, Y= H, 92, 17**	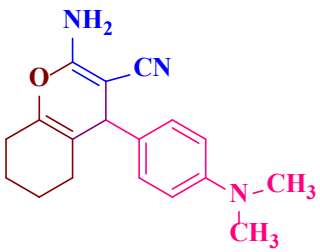 **4e: X= N,N dimethyl, Y= H, 93, 20**	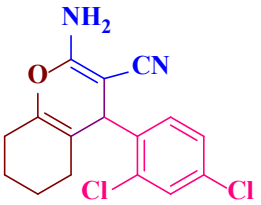 **4f: X=2,4 dichloro, Y= H, 91, 18**
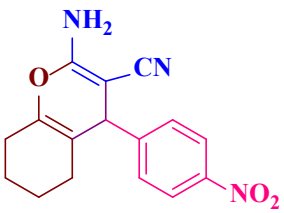 **4g: X= NO_2, Y= H, 94, 19**	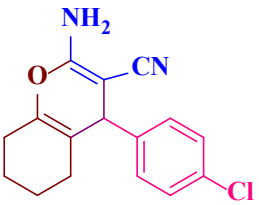 **4h: X= Cl, Y= H, 92, 17**	

[a] Reaction conditions: benzaldehyde (1 mmol), cyclohexanone (1 mmol), malononitrile (1 mmol), 0.1mmol nanocatalyst (5 mg), ethanol solvent (5ml), 45 power ultrasonic irradiation.
[b] Isolated yield

Table 5.
Comparisons of literatures reported catalyst with this work for synthesis compound 4a

Entry	Catalyst	Loading	Time (min)	Yield (%)	Method	Ref.
1	Morpholine	0.1 mmol	30	90	Reflux	[48]
2	$CaMgFe_2O_4$	0.1 mmol	20	92	r.t	[47]
3	$CoFe_2O_4$/lamellar mesopore silica/melamine	10 Mg	20	93	r.t	[31]
4	$NiFe_2O_4$/mesopore silica/guanidine	10 Mg	10	98	Ultrasound	This work

included various steps, at the first step, benzaldehyde and malononitrile reacted under Michael addition and formation the intermediate A under the nanomagnetic base $NiFe_2O_4$/mesopore silica/guanidine nanocatalyst. Then the cyclohexanone under condensation reaction joins to the intermediate A and formation intermediate B. The process followed by a cyclization reaction, the 4H-chromene (4a) compounds synthesis by absorption of the hydrogen, and double bonds rearrangement (Scheme 3).

3.2. Catalytic comparisons

To display the efficiency and influence of new methods for the synthesis of 4H-chromene derivatives, the obtained results were compared with the other methods, catalysts, and conditions (Table 5). As can be seen, the present study with different methods for added the starting material, nanocatalyst, and using ultrasonic irradiation is superior in yield of pure products and short reaction times.

3.3. Reusability

The reusability and nanocomposite are important advantages for commercial utilization. The reusability of $NiFe_2O_4$/mesopore silica/ guanidine nanocatalyst, was tested in six runs of the model reaction, and the results reported in Fig 8.

4. Conclusion

In this study, it was functionalized the $NiFe_2O_4$/mesopore silica with the guanidine compound. The mesopore silica has a large area for functionalization on the surface and pore. The reaction of benzaldehyde, malononitrile, and cyclohexanone as the model reaction was selected for examined the catalyst activity. The 4H-chromene was synthesized by used $NiFe_2O_4$/mesopore silica/ guanidine as a nanocatalyst in the excellent yields and short reaction times. The nanocomposite identified by FT-IR, SEM, XRD, VSM, BET techniques, and the organic products recognize by the melting point, ^{1}H NMR, and FT-IR analyses.

Supporting Information

Experimental details, copies of ^{1}H and FT-IR and of products is available free of charge via the Internet here.

Acknowledgments

The authors are grateful to University of shahrekord for supporting this work by Grant No. 159148/92.

Conflict of interest

The authors declare that there is no conflict of interest.

REFERENCES

[1] I.I. Slowing, B.G. Trewyn, S. Giri, V.Y. Lin, Mesoporous silica nanoparticles for drug delivery and biosensing applications, Advanced Functional Materials 17(8) (2007) 1225-1236.
[2] S.-H. Wu, C.-Y. Mou, H.-P. Lin, Synthesis of mesoporous silica nanoparticles, Chemical Society Reviews 42(9) (2013) 3862-3875.
[3] Z. Li, J.C. Barnes, A. Bosoy, J.F. Stoddart, J.I. Zink, Mesoporous silica nanoparticles in biomedical applications, Chemical Society Reviews 41(7) (2012) 2590-2605.
[4] S. Egodawatte, A. Datt, E.A. Burns, S.C. Larsen, Chemical insight into the adsorption of chromium (III) on iron oxide/mesoporous silica nanocomposites, Langmuir 31(27) (2015) 7553-7562.
[5] R.R. Castillo, M. Vallet-Regí, Functional mesoporous silica nanocomposites: biomedical applications and biosafety, International Journal of Molecular Sciences 20(4) (2019) 929.
[6] L. Wei, N. Hu, Y. Zhang, Synthesis of polymer—mesoporous silica nanocomposites, Materials 3(7) (2010) 4066-4079.
[7] P. Xu, H. Yu, X. Li, Functionalized mesoporous silica for microgravimetric sensing of trace chemical vapors, Analytical chemistry 83(9) (2011) 3448-3454.
[8] M. Gao, J. Zeng, K. Liang, D. Zhao, B. Kong, Interfacial Assembly of Mesoporous Silica-Based Optical Heterostructures for Sensing Applications, Advanced Functional Materials 30(9) (2020) 1906950.
[9] R. Nechikkattu, C.-S. Ha, Temperature-responsive mesoporous silica nanoreactor with polymer gatings immobilized surface via a 'grafting-to'approach as peroxidase-like catalyst, Microporous and Mesoporous Materials 306 (2020) 110472.
[10] F.-C. Lin, J.I. Zink, Probing the local nanoscale heating mechanism of a magnetic core in mesoporous silica drug-delivery nanoparticles using fluorescence depolarization, Journal of the American Chemical Society 142(11) (2020) 5212-5220.
[11] A.F. Zarandi, H. Shirkhanloo, P. Paydar, A novel method based on functionalized bimodal mesoporous silica nanoparticles for efficient removal of lead aerosols pollution from air by solid-liquid gas-phase extraction, Journal of Environmental Health Science and Engineering 18(1) (2020) 177-188.
[12] W. Wang, Y. Chen, A. Chen, X. Ma, Composite particles with dendritic mesoporous-silica cores and nano-sized CeO_2 shells and their application to abrasives in chemical mechanical polishing, Materials Chemistry and Physics 240 (2020) 122279.
[13] S. Mohammadi, H. Naeimi, Synthesis of novel bis-spirooxindoles catalyzed by magnetic cobalt ferrite encapsulated MCM-41@ MgO as a solid base, Current Organic Synthesis 18(2)(2020) 214-224.
[14] A. Kazemzadeh, M.A. Meshkat, H. Kazemzadeh, M. Moradi, R. Bahrami, R. Pouriamanesh, Preparation of graphene nanolayers through surfactant-assisted pure shear milling method, Journal of Composites and Compounds 1(1) (2019) 22-26.
[15] S. Eskandarinezhad, R. Khosravi, M. Amarzadeh, P. Mondal, F.J.C. Magalhães Filho, Application of different Nanocatalysts in industrial effluent treatment: A review, Journal of Composites and Compounds 3(6) (2021) 43-56.
[16] Y. Wang, J. He, Y. Shi, Y. Zhang, Structure-dependent adsorptive or photocatalytic performances of solid and hollow dendritic mesoporous silica & titania nanospheres, Microporous and Mesoporous Materials 305 (2020) 110326.
[17] Q. Yu, T. Deng, F.-C. Lin, B. Zhang, J.I. Zink, Supramolecular assemblies of heterogeneous mesoporous silica nanoparticles to co-deliver antimicrobial peptides and antibiotics for synergistic eradication of pathogenic biofilms, ACS nano 14(5) (2020) 5926-5937.
[18] J.S. Schulze, J. Migenda, M. Becker, S.M. Schuler, R.C. Wende, P.R. Schreiner, B.M. Smarsly, TEMPO-functionalized mesoporous silica particles as heterogeneous oxidation catalysts in flow, Journal of Materials Chemistry A 8(7) (2020) 4107-4117.
[19] B. Van Gemert, Benzo and Naphthopyrans (Chromenes), Organic Photochromic and Thermochromic Compounds: Volume 1: Main Photochromic Families, Springer, Boston, MA, Boston, MA, USA, 2002, pp. 111-140.
[20] R. Pratap, V.J. Ram, Natural and synthetic chromenes, fused chromenes, and versatility of dihydrobenzo [h] chromenes in organic synthesis, Chemical reviews 114(20) (2014) 10476-10526.
[21] M. Costa, T.A. Dias, A. Brito, F. Proença, Biological importance of structurally diversified chromenes, European journal of medicinal Chemistry 123 (2016) 487-507.
[22] S.A. Patil, J. Wang, X.S. Li, J. Chen, T.S. Jones, A. Hosni-Ahmed, R. Patil, W.L. Seibel, W. Li, D.D. Miller, New substituted 4H-chromenes as anticancer agents, Bioorganic & Medicinal Chemistry Letters 22(13) (2012) 4458-4461.
[23] A.M.M. El-Saghier, M.B. Naili, B.K. Rammash, N.A. Saleh, K.M. Kreddan, Synthesis and antibacterial activity of some new fused chromenes, Arkivoc 16 (2007) 83-91.
[24] V.T. Angelova, Y. Voynikov, P. Andreeva-Gateva, S. Surcheva, N. Vassilev,

T. Pencheva, J. Tchekalarova, In vitro and in silico evaluation of chromene based aroyl hydrazones as anticonvulsant agents, Medicinal Chemistry Research 26(9) (2017) 1884-1896.
[25] N.M. Sabry, H.M. Mohamed, E.S.A. Khattab, S.S. Motlaq, A.M. El-Agrody, Synthesis of 4H-chromene, coumarin, 12H-chromeno [2, 3-d] pyrimidine derivatives and some of their antimicrobial and cytotoxicity activities, , European Journal of Medicinal Chemistry 46(2) (2011) 765-772.
[26] O.S. Patrusheva, V.V. Zarubaev, A.A. Shtro, Y.R. Orshanskaya, S.A. Boldyrev, I.V. Ilyina, S.Y. Kurbakova, D.V. Korchagina, K.P. Volcho, N.F. Salakhutdinov, Anti-influenza activity of monoterpene-derived substituted hexahydro-2H-chromenes, Bioorganic & Medicinal Chemistry 24(21) (2016) 5158-5161.
[27] A. Parthiban, J. Muthukumaran, A. Manhas, K. Srivastava, R. Krishna, H.S.P. Rao, Synthesis, in vitro and in silico antimalarial activity of 7-chloroquinoline and 4H-chromene conjugates, Bioorganic & Medicinal Chemistry Letters 25(20) (2015) 4657-4663.
[28] K. Takao, H. Yahagi, Y. Uesawa, Y. Sugita, 3-(E)-Styryl-2H-chromene derivatives as potent and selective monoamine oxidase B inhibitors, Bioorganic Chemistry 77 (2018) 436-442.
[29] M. Amirnejad, M.R. Naimi-Jamal, H. Tourani, H. Ghafuri, A facile solvent-free one-pot three-component method for the synthesis of 2-amino-4H-pyrans and tetrahydro-4H-chromenes at ambient temperature, Monatshefte für Chemie-Chemical Monthly 144(8) (2013) 1219-1225.
[30] S. Rostamnia, A. Nuri, H. Xin, A. Pourjavadi, S.H. Hosseini, Water dispersed magnetic nanoparticles (H_2O-DMNPs) of γ-Fe_2O_3 for multicomponent coupling reactions: a green, single-pot technique for the synthesis of tetrahydro-4H-chromenes and hexahydroquinoline carboxylates, Tetrahedron Letters 54(26) (2013) 3344-3347.
[31] S. Mohammadi, H. Naeimi, Functionalized $CoFe_2O_4$/lamellar mesopore silica anchored to melamine nanocomposite as a novel catalyst for synthesis of 4H-chromenes under mild conditions, Applied Organometallic Chemistry 34(6) (2020) e5630.
[32] L.N. Nasirmahale, F. Shirini, H. Tajik, O.G. Jolodar, Efficient Synthesis of 5-Oxo-5, 6, 7, 8-Tetrahydro-4H-Chromenes Assisted by Poly (4-Vinylpyridine), Polycyclic Aromatic Compounds 40(2)(2018) 475-483.
[33] R. Pourhasan-Kisomi, F. Shirini, M. Golshekan, Introduction of organic/inorganic Fe_3O_4@ MCM-41@ Zr-piperazine magnetite nanocatalyst for the promotion of the synthesis of tetrahydro-4H-chromene and pyrano [2, 3-d] pyrimidinone derivatives, Applied Organometallic Chemistry 32(7) (2018) e4371.
[34] J.M. Khurana, B. Nand, P. Saluja, 1, 8-Diazabicyclo [5.4. 0] undec-7-ene: A Highly Efficient Catalyst for One-Pot Synthesis of Substituted Tetrahydro-4H-chromenes, Tetrahydro [b] pyrans, Pyrano [d] pyrimidines, and 4H-Pyrans in Aqueous Medium, Journal of Heterocyclic Chemistry 51(3) (2014) 618-624.
[35] I. Hua, M.R. Hoffmann, Optimization of ultrasonic irradiation as an advanced oxidation technology, Environmental Science & Technology 31(8) (1997) 2237-2243.
[36] S.-i. Umemura, C.A. Cain, K. Katakura, Ultrasonic irradiation system, Google Patents, 1989.
[37] A. Kotronarou, G. Mills, M.R. Hoffmann, Ultrasonic irradiation of p-nitrophenol in aqueous solution, the journal of physical chemistry 95(9) (1991) 3630-3638.
[38] L. Saunders, J. Perrin, D. Gammack, Ultrasonic irradiation of some phospholipid sols, journal of physical chemistry 14(1) (1962) 567-572.
[39] F. Sharifianjazi, H. Pakseresht Amir, M. Shahedi Asl, A. Esmaeilkhanian, H. Nargesi khoramabadi, H. Won Jang, M. Shokouhimehr, Hydroxyapatite consolidated by zirconia: applications for dental implant, Journal of Composites and Compounds 2(2) (2020).
[40] X. Wang, J. Song, J. Liu, Z.L. Wang, Direct-current nanogenerator driven by ultrasonic waves, Science 316(5821) (2007) 102-105.
[41] J. Daraei, Production and characterization of PCL (Polycaprolactone) coated TCP/nanoBG composite scaffolds by sponge foam method for orthopedic applications, Journal of Composites and Compounds 2(2) (2020) 44-49.
[42] E. Asadi, A.F. Chimeh, S. Hosseini, S. Rahimi, B. Sarkhosh, L. Bazli, R. Bashiri, A.H.V. Tahmorsati, A review of clinical applications of graphene quantum dot-based composites, Journal of Composites and Compounds 1(1) (2019) 31-40.
[43] D.L. White, Amplification of ultrasonic waves in piezoelectric semiconductors, Journal of Applied Physics 33(8) (1962) 2547-2554.
[44] M.J. Lowe, Matrix techniques for modeling ultrasonic waves in multilayered media, IEEE Transactions on Ultrasonics, Ferroelectrics, and Frequency Control 42(4) (1995) 525-542.
[45] K.A. Nelson, R.D. Miller, D. Lutz, M. Fayer, Optical generation of tunable ultrasonic waves, Journal of Applied Physics 53(2) (1982) 1144-1149.
[46] S. Mohammadi, H. Naeimi, A synergetic effect of sonication with yolk-shell nanocatalyst for green synthesis of spirooxindoles, Green Chemistry Letters and Reviews 14(2) (2021) 344-356.
[47] H.K. Mohammadi, K.K. Kalantari, S.S. Naeimi, M. Pouretezad, E. Shokri, M. Tafazoli, M. Dastjerdi, L. Kardooni, Immediate and delayed effects of forearm kinesio taping on grip strength, Iranian Red Crescent Medical Journal 16(8) (2014) 3630-3638.
[48] H. Naeimi, S. Mohammadi, Synthesis of 1H-Isochromenes, 4H-Chromenes and Orthoaminocarbonitrile Tetrahydronaphthalenes by $CaMgFe_2O_4$ Base Nanocatalyst, ChemistrySelect 5(8) (2020) 2627-2633.